Fermi surface nesting in $Ba_{1-x}K_xBiO_3$ observed by Compton profile measurement

N. Hiraoka,* T. Buslaps, and V. Honkimäki
European Synchrotron Radiation Facility (ESRF), BP 220, 38043 Grenoble Cedex 9, France

H. Minami and H. Uwe
Institute of Materials Science, University of Tsukuba, Tsukuba, Ibaraki 305-8573, Japan
(Received 30 September 2004; revised manuscript received 21 January 2005; published 10 May 2005)

Compton profiles of $Ba_{1-x}K_xBiO_3$ have been measured, where $x=0.13$ and 0.39, to elucidate the relation between the Fermi surface and the metal-insulator transition. The two-dimensional momentum densities, reconstructed from several directional Compton profiles, are compared with those calculated by band theory. The momentum density of the $x=0.39$ metallic sample is explained by the predicted Fermi surface, except for one minor difference. Whereas, that of the $x=0.13$ insulating sample is simply reproduced by the geometry of the fcc-type Brillouin zone, suggesting the disappearance of the Fermi surface at the zone boundaries due to nesting. This result validates the interpretation that the insulating behavior of this system originates from the charge density wave instability.

DOI: 10.1103/PhysRevB.71.205106 PACS number(s): 71.18.+y, 31.15.Ar, 72.25.−b, 78.70.Ck

I. INTRODUCTION

The perovskite-type bismuth oxide, $Ba_{1-x}K_xBiO_3$, shows a complicated behavior dependent on the concentration of the potassium atoms.[1,2] Basically, the crystal structure is always (pseudo-) cubic. However, it is slightly distorted with various tilts and rotations of the BiO_6 octahedra as a function of x. At $x=0$, it is a monoclinic crystal, which possesses the ordered breathing-type distortion.[3,4] It transforms to an orthorhombic structure at $x\sim0.1$, showing the disordered distortion of the same type. It then transforms again to a simple cubic (sc) structure at $x\sim0.3$. Furthermore, it has recently been confirmed that the cubic phase also gradually transforms to a tetragonal structure with decreasing temperature.[5–7] Around this critical x (of $\sim$0.3), where the orthorhombic-cubic(tetragonal) structural transition happens, the sample shows the insulator-metal transition (insulating $\rightarrow$metallic, with increasing x). Just after this transition, it shows superconductivity with the highest critical temperature (T_c) of 31 K, and T_c goes down with increasing x.[8] Finally it reaches the solubility limit of $x\sim0.5$. It is widely believed that the insulator—metal transition at $x\sim0.3$ is due to the charge density wave (CDW) instability on the Fermi surface (FS). In order to verify this model, numerous experimental[1–7,9–11] and theoretical[12–19] studies have been carried out. In order to be able to discuss the CDW, knowledge of the FS is essential. Nevertheless, experimental elucidation for the FS is apparently insufficient for this material.

In principle, it is possible to investigate the FS evolution as a function of x, using de Haas van Alphen experiments and/or angle resolved photoemission spectroscopy, which are well established methods for FS studies. However, there are no reports of such a study of this material until now. The reason that these experiments have not been reported is probably the intrinsic difficulty in the preparation of perfect crystals and clean surfaces for these types of materials, caused by the doping atoms. The only experiment associated with FS study (except for a preliminary de Haas van Alphen experiment[20]) was conducted using the positron angular correlation of annihilation radiation (ACAR).[21] However, it reports only for one sample, where $x=0.4$, therefore it is difficult to find any relation between CDW (or the metal-insulator transition) and FS. It should be noted that ACAR is also sometimes limited by the sample quality.

An energy spectrum of Compton scattered x rays provides information about the electron momentum density distribution, projected onto the scattering vector, i.e., Compton profile (CP), $J(p_z)$ (see, e.g., Ref. 22)

$$J(p_z)=\int\int n(\mathbf{p})dp_xdp_y, \tag{1}$$

where p_z is the momentum component along the scattering vector, and $n(\mathbf{p})$ is the momentum density. The FS is defined as the boundary between occupied and unoccupied states in momentum space. Therefore, one can extract information about the FS by analyzing the momentum density distribution. The advantage of this method is that, due to the large x-ray penetration depth of 100–1000 μm in a sample, it is not limited by the sample quality and it probes the bulk. Furthermore, Compton scattering detects FS signals at any point in the momentum space, even beyond the first Brillouin zone (BZ), as well as the ACAR. The integration of the momentum density along the p_x and p_y axes makes intuitive understanding difficult. However, the three-dimensional (3D) momentum density, $n(\mathbf{p})$, or the (projected) 2D momentum density can be determined by a numerical reconstruction method with the several directional CPs (see Sec. III). In this study, we have obtained the projected 2D momentum densities on the (001) plane using the 2D reconstruction method from several directional CPs for $Ba_{0.61}K_{0.39}BiO_3$ and $Ba_{0.87}K_{0.13}BiO_3$. Based on a comparison with a theory, which has previously been reported, we conclude that the obtained electron momentum density distributions represent the FS nesting.

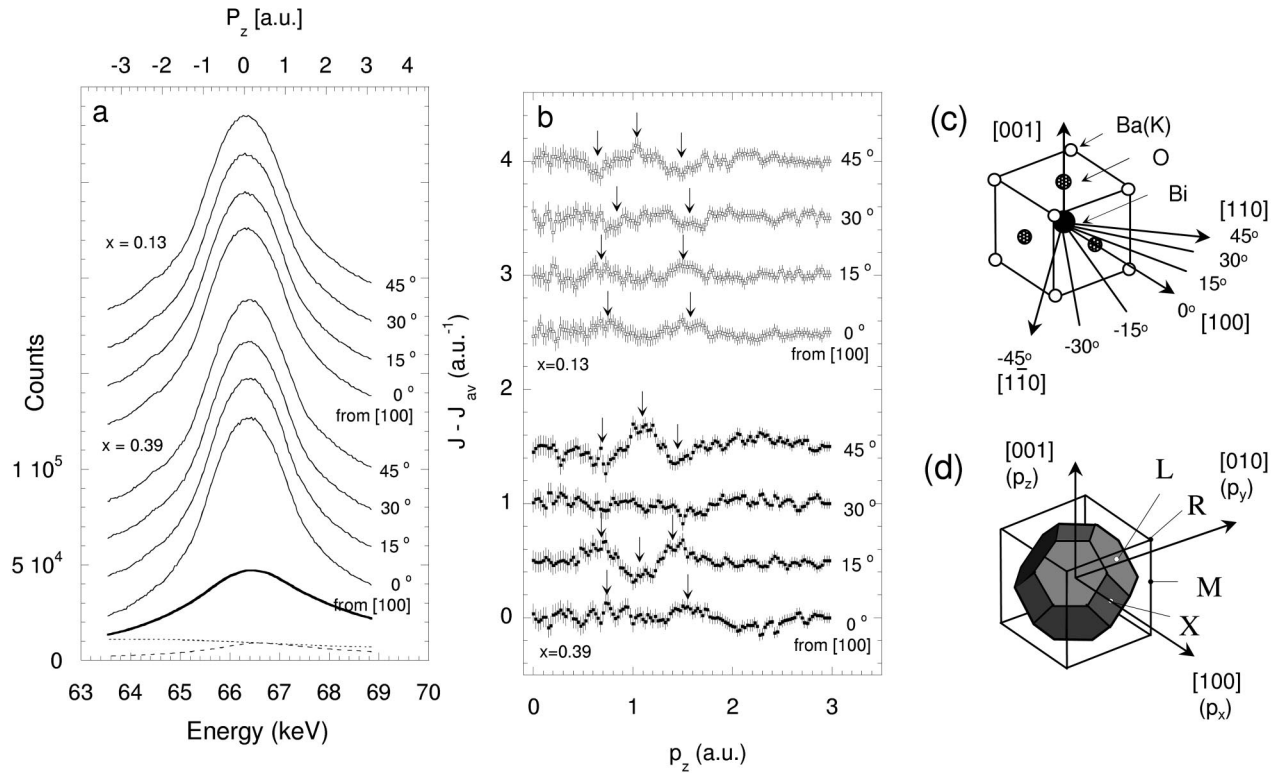

FIG. 1. (a) Raw spectra of $x=0.39$ and $x=0.13$ samples (solid lines). Contributions of core electrons (thick, solid line), the multiple (double+triple) scattering components (broken line), and the background (dotted line) are shown only for the $x=0.39$ sample along the [100] axis. Spectra are shifted, in the y-direction, from the previous spectrum by 20 000 counts. (b) Anisotropic components of CPs, $J-J_{\mathrm{av}}$, where J_{av} are the average of 4 CPs on each sample. Spectra are shifted, in the y-direction, from the previous spectrum by 0.5. Error bars represent the statistical accuracy. Discernible signals are marked by arrows. (c) Experimental geometry. Bi—O bonding directions are taken as ⟨100⟩. (d) Geometries of the first BZs in the nondistorted phase (solid lines) and the distorted phase (gray surfaces).

II. EXPERIMENTS

The samples, typically having a size of $\sim 2^3$ mm^3, were prepared by the electrochemical method.[23,24] The Compton scattering experiments were carried out with a dispersion-compensation type spectrometer[25] on ID15B at the European Synchrotron Radiation Facility. An incident photon energy of 88.3 keV was chosen, which is just below the K-edge of Bi. The beam size was 5 (vertical) $\times$ 2(horizontal) mm^2. In order to obtain a higher count rate, the two crystals, whose orientations were verified by Laue photographs, were positioned vertically. Since the sample is expected to have a 3D-FS, the 3D reconstruction is the best method. It is clear that the more directional CPs would be better for the reconstruction procedure. However, it is also necessary to take a long exposure time for one directional CP so as to improve statistical accuracy to detect small FS signals. A compromise must be made in order to reach a meaningful conclusion. As for $Ba_{1-x}K_xBiO_3$, the angular dispersions of the FSs are expected to be small, while the FS signals are anticipated to be very weak, due to very small numbers of electrons (0.61 and 0.87 per unit cell) which are relevant to the FS, compared to the total electron numbers (148.57 and 158.19). We measured 7 directional CPs between [110] and [1$\bar{1}$0] for the 2D reconstruction on the (001) plane, and then summed the two equivalent directional CPs in the sc representation [e.g., −15° and 15° in Fig. 1(c)] after confirming their identity. By adopting the 2D reconstruction instead of the 3D one, the number of CPs can be reduced to $\sim\sqrt{N}$ with a similar accuracy, where N is the number of CPs which is necessary for the 3D reconstruction, while it still provides rich information.[26] The $\sim$100 000 counts were accumulated at the peak of CPs in a bin of $\sim$0.025 atomic units (a.u.: 1 a.u. $=1.99\times10^{-24}$ kg m s^{-1}) for each (summed) CP. The momentum resolution varied between 0.10 and 0.14 a.u. depending on the sample orientation. The double and triple scattering contributions were evaluated to be 7.18% and 0.46% using the program developed by Fajardo *et al.*[27]

Figure 1(a) shows the raw spectra along with contributions from the core electron,[28] the multiple scattering and the background. Here, Ba$(1s)^2$-$(4p)^6$, K$(1s)^2$-$(3p)^6$, Bi$(1s)^2$-$(5d)^{10}$ and O$(1s)^2$ electrons are regarded as the core electrons. It is typical for Compton scattering to observe almost isotropic spectra, showing no prominent structures. The most popular way to make valence or conduction contributions visible is to take the difference between two spectra measured along different crystal orientations. This exhibits anisotropic contributions from valence and/or conduction electrons. Figure 1(b) shows the anisotropies of the CPs, $J-J_{\mathrm{av}}$, where J_{av} are obtained by averaging 4 CPs for each sample. There are several discernible structures on the $J-J_{\mathrm{av}}$ (marked by arrows in the figure). The two samples show similar be-

haviors to each other. The $x=0.13$ sample shows a smaller anisotropy than the $x=0.39$ sample on the 15° and 45° spectra, while it shows larger anisotropy on the 30° spectrum. Even though we find the x-dependent, anisotropic components of CPs, it is difficult to discuss the FS evolution because: (i) the origins of these signals are unclear due to the double integral of the momentum density [Eq. (1)], and (ii) the anisotropies can arise from the other contributions, e.g., bonding orbitals between Bi(Ba, K) and O atoms,[29] as well as the FS geometry. It was also tried to take the difference between the CPs of the $x=0.13$ sample and the $x=0.39$ one along each axis. However, the differences were quite small and the FS signals were still unclear (not shown). In order to be able to discuss the FSs, the reconstruction and the folding procedure are essential to isolate the FS signals from the other contributions, as discussed below.

III. RECONSTRUCTION AND LCW FOLDING

The direct Fourier transformation method was used for the reconstruction. This reconstruction is generally carried out as follows. We first define the so-called $B(\mathbf{r})$-function as the 3D Fourier transformation of the momentum density, $n(\mathbf{p})$, i.e.,

$$B(\mathbf{r}) = \int\int\int n(\mathbf{p})\exp(-i\mathbf{p}\cdot\mathbf{r})d\mathbf{r}. \tag{2}$$

Conversely, the $n(\mathbf{p})$ is given as,

$$n(\mathbf{p}) = (2\pi)^{-3}\int\int\int B(\mathbf{r})\exp(i\mathbf{r}\cdot\mathbf{p})d\mathbf{r}. \tag{3}$$

From Eqs. (1) and (2), we find that

$$B(0,0,z) = \int J(p_z)\exp(-ip_z z)dp_z: \tag{4}$$

Namely, the $B(\mathbf{r})$ is simply given by the Fourier transformation of the Compton profile on each axis. Once we perform the 3D interpolation of the $B(\mathbf{r})$ for all of real space [up to points where $B(\mathbf{r})=0$], it is possible to carry out the inverse 3D-Fourier transformation of the $B(\mathbf{r})$ based on Eq. (3), so as to obtain the 3D momentum density. In this study, a 2D reconstruction was performed. The 2D reconstruction provides the projected momentum density onto the p_x-p_y plane. The conversion to the 2D reconstruction is straightforward. Eq. (3) is simply converted to

$$n_{2D}(p_x,p_y) = \int n(\mathbf{p})dp_z = (2\pi)^{-2}\int\int B(x,y,0)\exp(ixp_x+iyp_y)dxdy. \tag{5}$$

$B(x,y,0)$ is obtained by the Fourier transformation of Compton profiles and the 2D interpolation, similar to the procedure in the 3D reconstruction. Note here that the scattering axes are customarily taken in the p_x-p_y plane, unlike in Eq. (1).

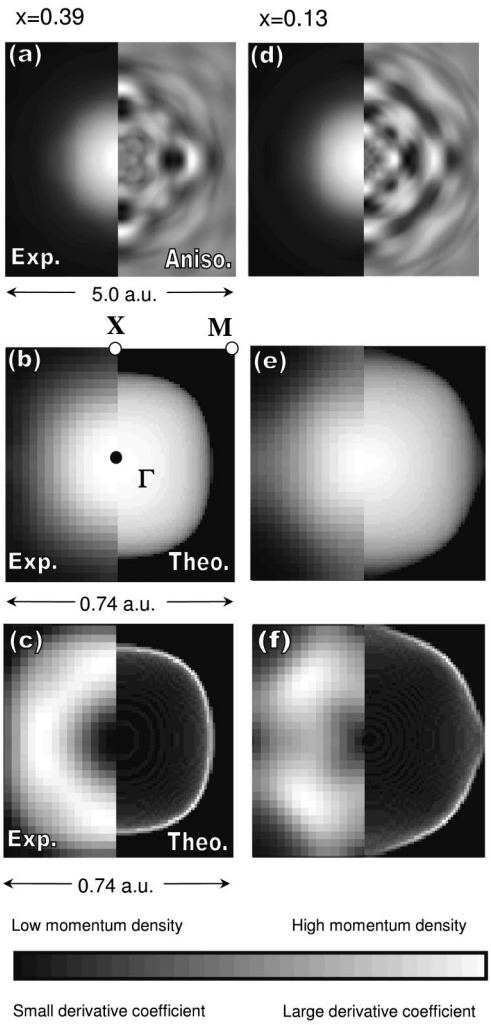

FIG. 2. (a) and (d) Reconstructed 2D momentum densities (left sides) and their anisotropic components (right sides) for the $x=0.39$ sample and the $x=0.13$ samples. (b) and (e) LCW-folded momentum densities (left), compared to band theory (right). (c) and (f) Derivatives of the LCW-folded momentum densities.

The program developed by Tanaka *et al.* was used[30] for the reconstruction. Except for the dimensionality, this is basically the same as the program described in detail in Ref. 31.

Figure 2(a) shows the reconstructed 2D-momentum density (left side) and its anisotropic component (right side) of the $x=0.39$ sample, where the latter is obtained by subtracting the isotropic component from the former. Even after the reconstruction, it is still difficult to recognize FS signals. Therefore, we have adopted the Lock-Crisp-West folding method (LCW folding),[32] which folds the momentum density into the first BZ using reciprocal lattice vectors. The LCW folding enhances periodic signals with respect to the reciprocal lattice vectors while it suppresses other signals. Figure 2(b) shows the folded 2D-momentum density (left side) of the $x=0.39$ sample and it is compared with LDA band theory (right side). The theoretical result is obtained just by the p_z-axis projection of the electron density inside the FS, reproduced from the FS parameters of Sahrakorpi *et al.*.[18] This calculation only provides FS effects and includes no other

contributions, i.e. wave function effects, and also the broadening effect due to the experimental resolution. The reasonable agreement between the theory and the experiment allows for us to regard that the LCW-folded momentum density represents the contributions from the FS.[34,35] This study is not the only case where the FS signals are drastically enhanced by the folding. The ACAR experiment[21] observed a similar enhancement on this kind of sample. Furthermore, our Compton scattering experiments on a molybdenum oxide[36] and a ruthenium oxide[37] also show a similar enhancement.

Figure 2(c) shows the derivatives of the folded 2D-momentum densities. Generally, when a 2D reconstruction method is applied to 3D samples, the derivative does not provide the correct positions of the FS, unlike a 3D reconstruction method. However, the derivative of the theoretical 2D momentum density exhibits the clear FS on the (001) plane as seen in Fig. 2(c) (right side), because the 2D momentum density rapidly drops near these positions [see Fig. 2(b), right]. Unfortunately, our experimental resolution, which is typical for Compton scattering experiments, is not high enough to resolve such a feature [Fig. 2(c), left]. Nevertheless, the derivative is still useful for making close comparisons. The same analysis has been carried out for the $x=0.13$ sample [see Figs. 2(d)–2(f)]. The difference between the experiment and the theory will be discussed below.

IV. RESULTS AND DISCUSSION

Figure 3 shows comparisons between the experimental and theoretical LCW-folded 2D momentum densities. For a complete comparison, the theoretical 2D momentum densities were obtained as follows: First the 3D momentum densities were calculated from the FS parameters of Sahrakorpi *et al.*[18] as before. Then its 1D projections, i.e., $J(p_z)$s, were computed based on Eq. (1) along the four directions, where the experimental CPs were collected. Finally, the reconstruction and the LCW-folding were performed in the same way as the data analysis so as to obtain the 2D momentum densities. The reconstruction procedure included the broadening effect, corresponding to the experimental resolution, as a filtering function in the Fourier transformation. Note again that the theory only provides the contribution of the FS. As for the $x=0.39$ sample, the experimental result is explained by the theory except for one minor difference, i.e., a structure near L's seen in the derivative. Such a feature is also recognizable in the ACAR data.[21] This difference is discussed at the end of this section.

On the other hand, for $x=0.13$ sample, it is disputable whether or not the experimental momentum density can be compared with the theory because, (i) the real sample deviates from the cubic structure assumed by the theory, causing the BZ geometries to differ, and because (ii) the sample shows an insulatorlike behavior although the theory assumes the metallic phase. Reference 18 has provided a sensible discussion to justify this comparison, which is interpreted as follows. Since the metal-insulator transition accompanies the cubic-orthorhombic structural transition, the BZ also changes its shape from cubic-type to fcc-type.[33] The corners of the

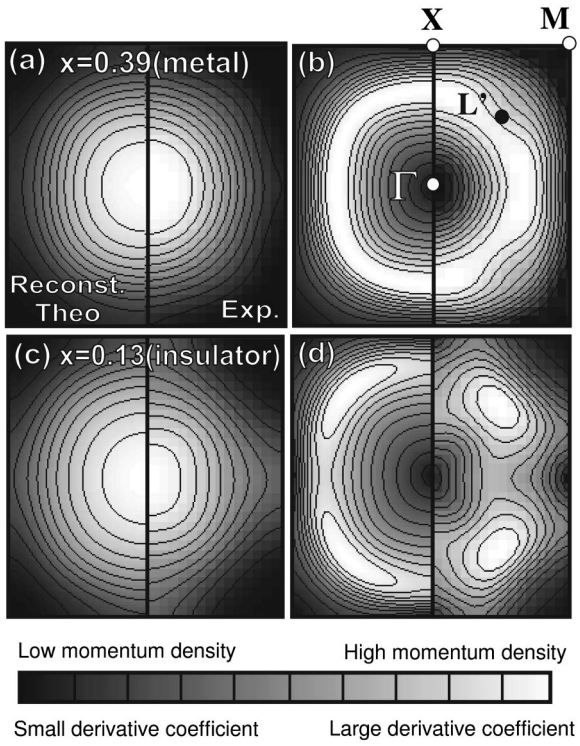

FIG. 3. Comparisons between theory and experiment for the $x=0.39$ sample [(a) momentum density and (b) derivative] and the $x=0.13$ sample [(c) momentum density and (d) derivative]. L' is the projection of L onto the (001) plane.

cubic BZ, i.e., R points are replaced by new Γ points, and then they make new additional FSs there. However, such a process is never strong because the orthorhombic structure is provided only by a very small lattice distortion. Therefore one can uphold the assumption that the BZ is cubic. Apart from this, in an insulator state, the discontinuity in the momentum density (Fermi break), which defines FS, is smeared out in the momentum range of $\sim E_g/v_F$. Here, E is the energy gap and v_F is the Fermi velocity of the associated metallic state, which can be defined as the gradient of the E-k curve at the Fermi energy in the band structure diagram. If the insulating behavior of the sample originates from the small gap, the FS is smeared only in a small range, which may be much smaller than the experimental resolution. Hence such a "pseudo" FS may be detected by the experiments. Here, even if we assume the large gap of 2 eV (corresponding to ~0.15 a.u. broadening), which is observed by optical measurements,[9] this interpretation does not change. This momentum broadening, slightly larger than the present resolution, is not so large as to completely smear out the FS geometry.

Nevertheless, the present experimental result shows the two crucial differences from the theoretical result. Basically, both the experimental and the theoretical results are interpreted as the expansion of the FS due to the increase of the number of electrons as x decreases. Firstly, however, the experimental momentum density of the $x=0.13$ sample seems to be in contact with BZ boundaries at Xs, much more than the theory suggests. Secondly, the experimental momentum

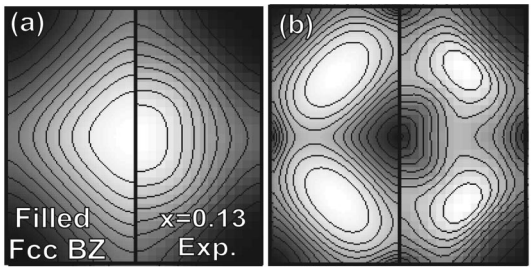

FIG. 4. Comparisons between the 2D-momentum density (a) [the derivative (b)] of the filled fcc-type BZ and the experimental results on the $x=0.13$ sample.

density of the $x=0.13$ sample shows a squarelike shape, rotated by 45° from the [100] axis, in contrast to the round shape in the $x=0.39$ sample. This feature is not seen in the theory. Those features are more emphasized in the derivative image. As a model to explain these features, we suggest the momentum density distribution which fills the fcc-type BZ for the $x=0.13$ sample, i.e., FS which coincides with the fcc-type zone boundaries [see, Fig. 1(d)]. This model is obtained by considering that the FS expansion is impeded on {111} planes. In order to confirm this model, we have computed the 1D projection of the fcc-type BZ (without considering any FS effect), and then reconstructed the 2D momentum density in the same manner as before. Figure 4 shows the result. It shows a very good agreement with the experimental result, indicating the validity of this model. This momentum density distribution is closely associated to the emergence of the CDW and/or the CDW-derived structural transition. The CDW consists of Bi^{3+} and Bi^{5+}, indexed by the $\sqrt{2}\times\sqrt{2}\times2$-type orthorhombic structure. Since this CDW makes an energy gap at the boundaries of the fcc-type BZ, the electrons near the FS gain a lot of energy and the FS disappears once the CDW appears (Hume-Rothery mechanism). The present result clearly depicts how the FS evolution leads to the CDW instability.

As often discussed so far, it is only possible for the $x=0$ sample, possessing a half-filled Bi $6s$—O $2p$ band, to have a complete nesting. While, the $x=0.13$ sample has to have small hole pockets somewhere in the fcc-type BZ, according to Luttinger theorem. The sample, therefore, is expected to be a low-carrier metal with a pseudo gap. This expectation is contradicted by the insulating behavior of the sample. This issue is in common with a question, which has been discussed for 20 years and has not been completely solved yet: why do the insulator phases in $Ba_{1-x}K_xBiO_3$ and $BaPb_{1-x}Bi_xO_3$ extend in wide K(Pb) concentration ranges? In order to explain this, various theoretical models are proposed.[12–14,16,17,19] It is difficult to examine them with this result because, first, those theories show no clear prediction for the FS geometry or the electron distribution in k-space (i.e., momentum distribution), and secondly, fine structures associated with the FS are lost in our experimental results. We may be able to argue, however, that our data support the (bi)polaron model in Ref. 19. In this model, a hole moves between two different sites of Bi, which have different valencies (charge disproportionation) and also different Bi—O distances. Since the hole itself changes the valencies and Bi—O distances, a hole is expected to become (bi)polarons with quite low mobility. Such a localized carrier could escape from the detection of the Compton scattering experiment, because it would have a spread momentum distribution. With increasing x, the charge disproportionation becomes smaller, and thus the polaron effect also becomes less significant. This explains why LDA band theory reproduces the data on the $x=0.39$ sample, but not for the $x=0.13$ sample.

Finally, we briefly discuss the minor difference between the theory and the experiment for the $x=0.39$ metallic sample. The main feature of the data of the $x=0.13$ sample is a strong drop off in the momentum density near L'-points. This feature is not prominent for the $x=0.39$ sample but an unusual structure is still recognizable at same the positions [Fig. 3(b)]. This might be due to the gap opening around L-points even in this metallic sample. This interpretation is consistent with the reports of optical measurements[9,10] and angle-integrated photo-emission spectroscopy,[11] which have observed a remnant CDW signature and a pseudogap in metallic samples, respectively. This may arise from the tetragonal distortion, found by neutron diffraction at low temperature. The tetragonal structure can also lead to the CDW instability because it still has fcc-type BZ, as well as the orthorhombic structure. It is reported that the $x=0.39$ sample has a cubic structure at room temperature, but the tetragonal distortion might remain locally.

V. SUMMARY

We carried out the Compton scattering 2D-reconstruction experiments on $Ba_{1-x}K_xBiO_3$ so as to elucidate the relation between the FS and the CDW instability. The FS signals were unclear on the Compton profiles themselves, but the clear FS signals were detected on the reconstructed momentum densities with the folding procedure. The 2D momentum density in the $x=0.39$ sample was explained by the FS based on band theory. Whereas, the 2D momentum density in the $x=0.13$ sample was simply explained by the geometry of the fcc-type BZ. The present study has experimentally confirmed the FS nesting in the $x=0.13$ insulating sample. The other significance of this report is that the feasibility of Compton scattering experiments is shown for the CDW-derived transition. This method is particularly powerful when neither high quality sample nor clean surface is available because no other experiment shows FS.

ACKNOWLEDGMENTS

We would like to thank Y. Tanaka for providing the reconstruction program. We are also grateful to M. Shizuya for useful discussions.

*Electronic address: hiraoka@spring8.or.jp; present address: Taiwan BL, SPring-8, Mikazuki, Sayo, Hyogo, 679-5198, Japan.

[1] S. Pei, N. J. Zaluzec, J. D. Jorgensen, B. Dabrowski, D. G. Hinks, A. W. Mitchell, and D. R. Richards, Phys. Rev. B **39**, 811 (1989).
[2] S. Pei, J. D. Jorgensen, B. Dabrowski, D. G. Hinks, D. R. Richards, A. W. Mitchell, J. M. Newsam, S. K. Sinha, D. Vaknin, and A. J. Jacobson, Phys. Rev. B **41**, 4126 (1990).
[3] S. M. Heald, D. DiMarzio, M. Croft, M. S. Hegde, S. Li, and M. Greenblatt, Phys. Rev. B **40**, 8828 (1989).
[4] S. Salem-Sugui, E. E. Alp, S. M. Mini, M. Ramanathan, J. C. Campuzano, G. Jennings, M. Faiz, S. Pei, B. Dabrowski, Y. Zheng D. R. Richards, and D. G. Hinks, Phys. Rev. B **43**, 5511 (1991).
[5] A. P. Menushenkov, K. V. Klement'ev, P. V. Konarev, and A. A. Meshkov, JETP Lett. **67**, 1034 (1998).
[6] M. Braden, W. Reichardt, E. Elkaim, J. P. Lauriat, S. Shiryaev, and S. N. Barilo, Phys. Rev. B **62**, 6708 (2000).
[7] L. A. Klinkova, M. Uchida, Y. Matsui, V. I. Nikolaichik, and N. V. Barkovskii, Phys. Rev. B **67**, 140501(R) (2003).
[8] D. G. Hinks, B. Dabrowski, J. D. Jorgensen, A. W. Mitchell, D. R. Richards, S. Pei, and D. Shi, Nature (London) **333**, 836 (1988).
[9] S. H. Blanton, R. T. Collins, K. H. Kelleher, L. D. Rotter, Z. Schlesinger, D. G. Hinks, and Y. Zheng, Phys. Rev. B **47**, 996 (1993).
[10] M. E. Kozlov, X. Ji, H. Minami, and H. Uwe, Phys. Rev. B **56**, 12 211 (1997).
[11] A. Chainani, T. Yokoya, T. Kiss, S. Shin, T. Nishio, and H. Uwe, Phys. Rev. B **64**, 180509(R) (2001).
[12] T. M. Rice and L. Sneddon, Phys. Rev. Lett. **47**, 689 (1981).
[13] D. Yoshioka and H. Fukuyama, J. Phys. Soc. Jpn. **54**, 2996 (1985).
[14] E. Jurczek and T. M. Rice, Europhys. Lett. **1**, 225 (1986).
[15] L. F. Mattheiss and D. R. Hamann, Phys. Rev. Lett. **60**, 2681 (1988).
[16] C. M. Varma, Phys. Rev. Lett. **61**, 2713 (1988).
[17] A. Taraphder, H. R. Krishnamurthy, R. Pandit, and T. V. Ramakrishnan, Phys. Rev. B **52**, 1368 (1995).
[18] S. Sahrakorpi, B. Barbiellini, R. S. Markiewicz, S. Kaprzyk, M. Lindroos, and A. Bansil, Phys. Rev. B **61**, 7388 (2000).
[19] I. B. Bischofs, V. N. Kostur, and P. B. Allen, Phys. Rev. B **65**, 115112 (2002).
[20] R. G. Goodrich, C. Grienier, D. van Hall, A. Lacerda, E. G. Haanappel, D. Rickel, T. Northington, R. Schwarz, F. M. Mueller, D. D. Koelling, J. Vuillemin, L. Van-Bockstal, M. L. Norton, and D. H. Lowndes, J. Phys. Chem. Solids **54**, 1251 (1993).
[21] W. D. Mosley, J. W. Dykes, R. N. Shelton, P. A. Sterne, and R. H. Howell, Phys. Rev. Lett. **73**, 1271 (1994).
[22] M. J. Cooper, Rep. Prog. Phys. **48**, 415 (1985).
[23] H. Minami, T. Nishio, and H. Uwe, Adv. in Supercond. VIII (Proc. 8th ISS'95 Hamamatsu) p. 429 (1996).
[24] T. Nishio, H. Minami, and H. Uwe, Physica C **357–360**, 376 (2001).
[25] P. Suortti, T. Buslaps, M. DiMichiel, V. Honkimäki, U. Lienert, J. E. McCarthy, J. M. Merino, and A. Shukla, Nucl. Instrum. Methods Phys. Res. A **467**, 1541 (2001).
[26] G. Kontrym-Sznajd, R. N. West, and S. B. Dugdale, Mater. Sci. Forum **255**, 796 (1997).
[27] P. Fajardo, V. Honkimäki, T. Buslaps, and P. Suortti, Nucl. Instrum. Methods Phys. Res. B **134**, 337 (1998).
[28] F. Biggs, L. B. Mendelsohn, and J. B. Mann, *Atomic Data and Nuclear Data Tables* (Academic, New York, 1975), Vol. 16, p. 201.
[29] A. Shukla, B. Barbiellini, A. Erb, A. Manuel, T. Buslaps, V. Honkimäki, and P. Suortti, Phys. Rev. B **59**, 12 127 (1999).
[30] Y. Tanaka, K. J. Chen, C. Bellin, G. Loupias, H. M. Fretwell, A. Rodrigues-Gonzalez, M. A. Alam, S. B. Dugdale, A. A. Manuel, A. Shukla, T. Buslaps, P. Suorti, and N. Shiotani, J. Phys. Chem. Solids **61**, 365 (2000).
[31] Y. Tanaka, Y. Sakurai, A. T. Stewart, N. Shiotani, P. E. Mijnarends, S. Kaprzyk, and A. Bansil, Phys. Rev. B **63**, 045120 (2001).
[32] D. G. Lock, V. H. C. Crisp, and R. N. West, J. Phys. F: Met. Phys. **3**, 561 (1973).
[33] L. F. Mattheiss and D. R. Hamann, Phys. Rev. B **28**, 4227 (1983).
[34] J. H. Kaiser, R. N. West, and N. Shiotani, J. Phys. F: Met. Phys. **16**, 1307 (1986).
[35] Reference 34 shows that LCW folded momentum densities should include no wave function effects in the framework of the Korringer-Kohn-Rostoker (KKR) band theory.
[36] N. Hiraoka, T. Buslaps, V. Honkimäki, H. Guyot, and C. Schlenker, Phys. Rev. B **71**, 125417 (2005).
[37] N. Hiraoka, T. Buslaps, V. Honkimäki, M. Itou, Y. Sakurai, Z. Q. Mao, and Y. Maeno (unpublished).